A convective vorticity vector associated with tropical convection: A two-dimensional cloud-resolving modeling study

Shouting Gao and Fan Ping

Laboratory of Cloud-Precipitation Physics and Severe Storms (LACS), Institute of Atmospheric Physics, Chinese Academy of Sciences, Beijing, China

Xiaofan Li

Joint Center for Satellite Data Assimilation and National Oceanic and Atmospheric Administration National Environmental Satellite Data and Information Service Office of Research and Applications, Camp Springs, Maryland, USA

Wei-Kuo Tao

Laboratory for Atmospheres, NASA Goddard Space Flight Center, Greenbelt, Maryland, USA

Received 24 March 2004; revised 13 May 2004; accepted 21 May 2004; published 24 July 2004.

[1] Although dry/moist potential vorticity ($(\vec{\xi} \cdot \nabla\theta_e)/\rho$) is a useful physical quantity for meteorological analysis, it cannot be applied to the analysis of two-dimensional (2-D) simulations. A new vorticity vector ($(\vec{\xi} \times \nabla\theta_e)/\rho$ (convective vorticity vector (CVV)) is introduced in this study to analyze 2-D cloud-resolving simulation data associated with 2-D tropical convection. The cloud model is forced by the vertical velocity, zonal wind, horizontal advection, and sea surface temperature obtained from the Tropical Ocean-Global Atmosphere (TOGA) Coupled Ocean-Atmosphere Response Experiment (COARE) and is integrated for a selected 10-day period. The CVV has zonal and vertical components in the 2-D x-z frame. Analysis of zonally averaged and mass-integrated quantities shows that the correlation coefficient between the vertical component of the CVV and the sum of the cloud hydrometeor mixing ratios is 0.81, whereas the correlation coefficient between the zonal component and the sum of the mixing ratios is only 0.18. This indicates that the vertical component of the CVV is closely associated with tropical convection. The tendency equation for the vertical component of the CVV is derived and the zonally averaged and mass-integrated tendency budgets are analyzed. The tendency of the vertical component of the CVV is determined by the interaction between the vorticity and the zonal gradient of cloud heating. The results demonstrate that the vertical component of the CVV is a cloud-linked parameter and can be used to study tropical convection. *INDEX TERMS:* 3314 Meteorology and Atmospheric Dynamics: Convective processes; 3329 Meteorology and Atmospheric Dynamics: Mesoscale meteorology; 3337 Meteorology and Atmospheric Dynamics: Numerical modeling and data assimilation; *KEYWORDS:* convective vorticity vector, tropical convection, 2-D cloud model

Citation: Gao, S., F. Ping, X. Li, and W.-K. Tao (2004), A convective vorticity vector associated with tropical convection: A two-dimensional cloud-resolving modeling study, *J. Geophys. Res.*, *109*, D14106, doi:10.1029/2004JD004807.

1. Introduction

[2] Because it is conserved in frictionless adiabatic flow in a dry atmosphere, potential vorticity is one of the most important dynamic/thermodynamic parameters. It has been studied to enhance the understanding of the genesis and development of weather systems for more than 6 decades since it was first introduced by *Ertel* [1942]. However, it is not conserved when clouds develop and release latent heat. Moist potential vorticity is thus introduced by replacing potential temperature with the equivalent potential temperature, which is conserved in frictionless moist adiabatic processes. Many studies have contributed to understanding the roles of dry and moist potential vorticity in the genesis and development of weather systems [e.g., *Bennetts and Hoskins*, 1979; *Emanuel*, 1979; *Danielsen and Hipskind*, 1980; *Thorpe*, 1985; *Hoskins and Berrisford*, 1988; *Xu*, 1992; *Montgomery and Farrell*, 1993; *Cao and Cho*, 1995; *Cho and Cao*, 1998; *Gao et al.*, 2002].

[3] However, this important physical parameter cannot be applied to the analysis of the two-dimensional (2-D) simulation data. Dry/moist potential vorticity can be expressed as $(\vec{\xi} \cdot \nabla\theta_e)/\rho$, where $\vec{\xi}$ is the absolute vorticity, θ is the potential temperature in dry air and equivalent potential temperature in moist air, ρ is the air density, and ∇ is the 3-D gradient operator. For 2-D x-z

0148-0227/04/2004JD004807

flows [e.g., *Tao and Simpson*, 1993; *Wu et al.*, 1998; *Li et al.*, 1999],

$$\vec{\xi} = \left(\frac{\partial u}{\partial z} - \frac{\partial w}{\partial x} + 2\Omega\cos\varphi\right)\vec{j} + 2\Omega\sin\varphi\,\vec{k}$$

and

$$\nabla\theta_e = \frac{\partial\theta_e}{\partial x}\vec{i} + \frac{\partial\theta_e}{\partial z}\vec{k},$$

where u and w are the zonal and vertical wind components, respectively, x and z are the zonal and vertical coordinates, respectively, and $\vec{i}$ and $\vec{k}$ are the unit vectors in the zonal and vertical coordinates, respectively ($\vec{j} = \vec{k} \times \vec{i}$). Ω is the angular speed of the Earth's rotation, and φ is the latitude.

$$\frac{\vec{\xi}\cdot\nabla\theta_e}{\rho} = \frac{2\Omega\sin\varphi}{\rho}\frac{\partial\theta_e}{\partial z}.$$

For 2-D, equatorial flows ($\varphi = 0$), $(\vec{\xi}\cdot\nabla\theta_e)/\rho = 0$. This demonstrates that the 2-D flows do not contribute to the dry/moist potential vorticity. The vertical component of planetary vorticity is ignored henceforth.

[4] The new vorticity vector in the 2-D x-z frame is

$$\frac{\vec{\xi}\times\nabla\theta_e}{\rho} = \frac{1}{\rho}\left(\frac{\partial\theta_e}{\partial z}\zeta\vec{i} - \frac{\partial\theta_e}{\partial x}\zeta\vec{k}\right), \quad (1)$$

where

$$\zeta = \frac{\partial u}{\partial z} - \frac{\partial w}{\partial x}$$

and θ_e is the equivalent potential temperature, $2\Omega\cos\varphi$ is much smaller than ζ as indicated in Figure 4a and is neglected in this study. The new vector $((\vec{\xi}\times\nabla\theta_e)/\rho)$ has zonal ($P_x = (\zeta/\bar{\rho})((\partial\theta_e)/\partial z)$) and vertical ($P_z = -(\zeta/\bar{\rho})((\partial\theta_e)/\partial z)$) components in the 2-D x-z frame. This new vector will be used to analyze 2-D tropical convection based on hourly data from a cloud-resolving simulation. It will be demonstrated that this is an important vector whose variation is closely associated with that of tropical convection. The model, forcing, and experiment are briefly described in the next section. In section 3, 2-D modeling data will be used to analyze the vorticity and equivalent potential temperature gradients, calculate$(\vec{\xi}\times\nabla\theta_e)/\rho$, derive its tendency equation, and examine the dominant processes responsible for its variation in the tropical, deep convective regime. The summary is given in section 4.

2. Model

[5] The cloud-resolving model used in this study was originally developed by *Soong and Ogura* [1980], *Soong and Tao* [1980], and *Tao and Simpson* [1993]. The 2-D-version of the model used by *Sui et al.* [1994, 1998] and further modified by *Li et al.* [1999] is what is used in this study. The governing equations and model setup can be found in the work of *Li et al.* [1999, 2002c]. Several 2-D cloud-resolving models have successfully simulated atmospheric thermodynamic profiles, cloud properties, and precipitation in the tropics during the Global Atmospheric Research Program Atlantic Tropical Experiment (GATE) [e.g., *Xu and Randall*, 1996; *Grabowski et al.*, 1996] and Tropical Ocean Global Atmosphere Coupled Ocean-Atmosphere Response Experiment (TOGA COARE) [e.g., *Wu et al.*, 1998; *Li et al.*, 1999, 2002a, 2002b, 2002c; *Li*, 2004].

[6] The model is forced by zonally uniform vertical velocity, zonal wind, and thermal and moisture advection based on 6-hourly TOGA COARE observations within the Intensive Flux Array (IFA) region (M. H. Zhang, personal communication, 1999). The calculations are based on a constrained, variational method applied to column-integrated budgets of mass, heat, moisture, and momentum as proposed by *Zhang and Lin* [1997]. Hourly sea surface temperature (SST) at the Improved Meteorological (IMET) surface mooring buoy (1.75°S, 156°E) [*Weller and Anderson*, 1996] is also imposed in the model. The model is integrated from 0400 LST 19 December 1992 to 0400 LST 29 December 1992 (10 days total). Figure 1 shows the time evolution of the vertical distribution of the large-scale, atmospheric vertical velocity and zonal wind and the time series of the SST during the 10-day period. In this model setup the horizontal boundary is periodic. The horizontal domain is 768 km with a horizontal grid resolution of 1.5 km. The vertical grid resolution ranges from about 200 m near the surface to about 1 km near 100 mb. The time step is 12 s.

3. Results

[7] Figure 2 shows the time evolution and zonal distribution of surface rain rates during the 10-day integration. Convection occurs after a half-day of integration and begins to organize after another half-day of integration. Surface rain rates exceed 25 mm h^{-1} during the integration. Convection moves rather slowly over the first 3 days due to minimal mean-layer zonal flow (Figure 1b); it later propagates eastward as westerly winds intensify.

[8] Figure 3 shows zonal-vertical cross sections of streamlines and the sum of the mixing ratios of cloud hydrometeors at 1800 and 2100 LST 21 December and 0000 LST 22 December 1992. In the zonal domain between 200 and 768 km, there are three strong convective systems at 1800 LST 21 December associated with surface rainfall. The convection centered around 600 km is the strongest with hydrometeor mixing ratios of more than 5 g kg^{-1} above the melting level. The streamlines show the circulations with upward motion are associated with the convection. Westerly winds prevail across the model domain below 600 mb. The convection between 200 and 350 km has no significant propagation and later weakens. The convective systems between 400 and 500 km and 600 and 650 km move very little in 6 hours. However, clouds between these two convective systems develop by 2100 LST 21 December. The two convective systems merge, and the convection centered at 600 km weakens by 0000 LST 22 December.

[9] The vorticity ζ and the zonal and vertical gradients of the equivalent potential temperature θ_e at 2100 LST 21 December 1992 are plotted in Figure 4. Large variations in the vorticity and zonal and vertical gradients of equiva-

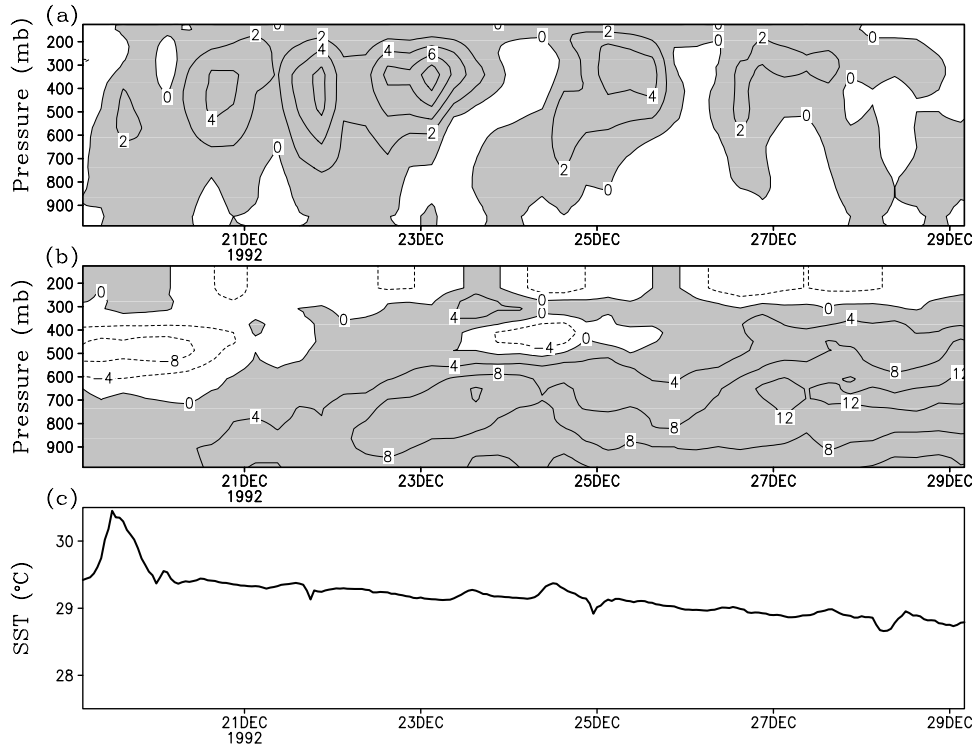

Figure 1. Temporal and vertical distribution of (a) vertical velocity, (b) zonal wind, and (c) time series of sea surface temperature observed and derived from Tropical Ocean-Global Atmosphere (TOGA) Coupled Ocean-Atmosphere Response Experiment (COARE) for the 10-day period. Upward motion in Figure 1a and westerly wind in Figure 1b are shaded. Units of vertical velocity, zonal wind, and sea surface temperature are cm s^{-1}, m s^{-1}, and °C, respectively.

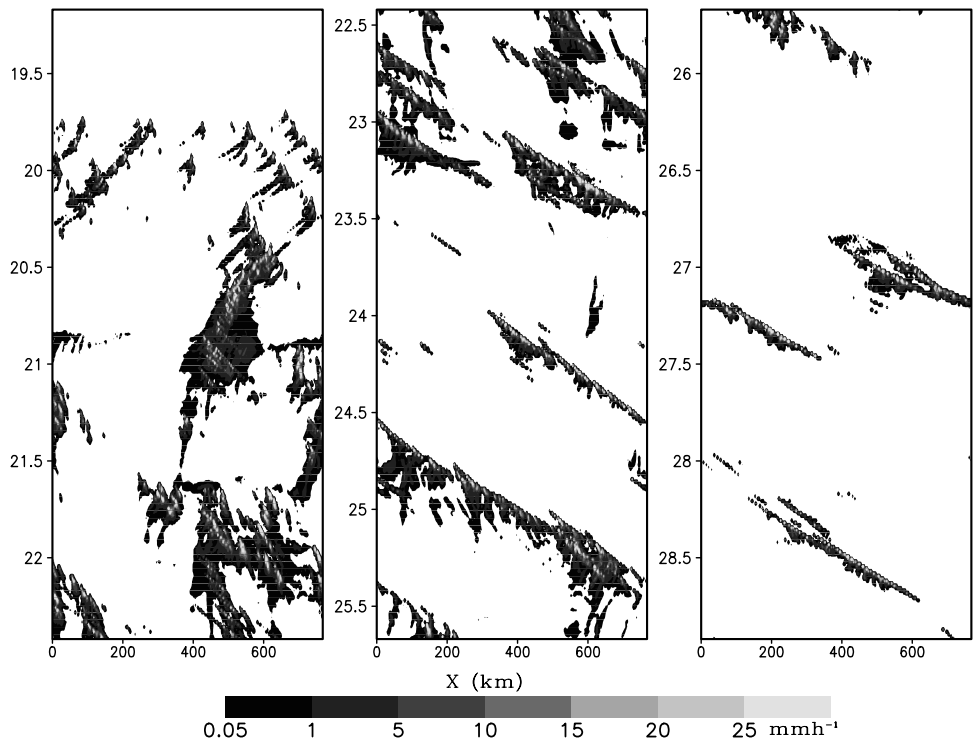

Figure 2. Temporal evolution and zonal distribution of surface rain rates (mm h^{-1}) from 19 to 29 December 1992.

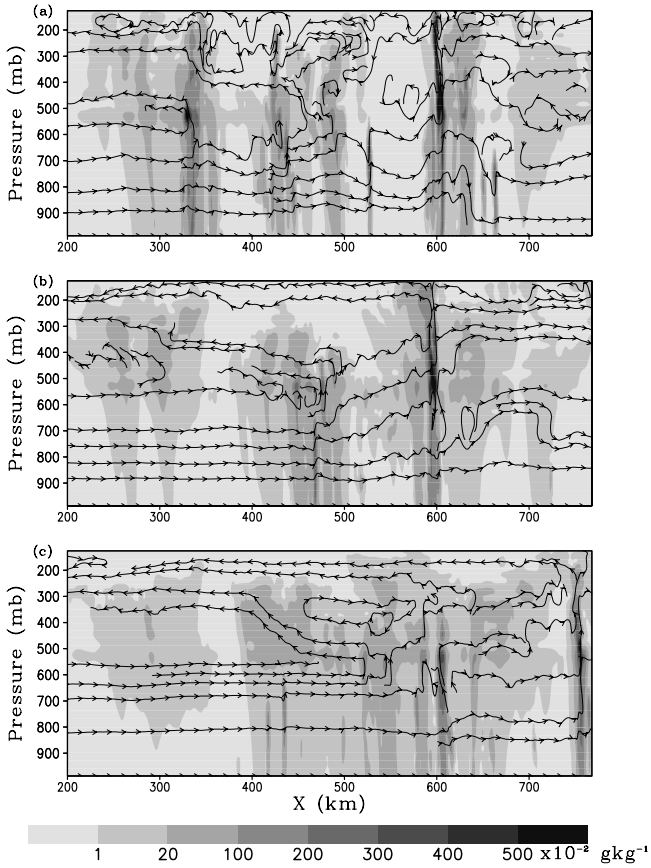

Figure 3. Zonal-vertical (X–Z) cross sections of streamlines and sum of the mixing ratios of cloud hydrometeors (background shading) at (a) 1800 LST, (b) 2100 LST 21, and (c) 0000 LST 22 December 1992.

lent potential temperature are associated with large magnitudes of hydrometeor mixing ratios, though the magnitudes of the zonal gradient are larger than those of the vertical gradient (note the difference in scale for the zonal and vertical gradients in Figures 4b and 4c). Thus both zonal (P_x) and vertical (P_z) components of $((\vec{\xi} \times \nabla\theta_e)/\rho)$ will be analyzed. As seen in the following analysis, the vector is closely associated with the variation of tropical clouds and is referred to as the convective vorticity vector (CVV).

[10] Zonally averaged and mass-integrated P_x, P_z, and sum of the cloud hydrometeor mixing ratios (i.e., q_c, q_r, q_i, q_s, q_g, the mixing ratios of cloud water (small cloud droplets), raindrops, cloud ice (small ice crystals), snow (density 0.1 g cm^{-3}), and graupel (density 0.4 g cm^{-3}), respectively) were calculated to examine their relationship. They are denoted by $[P_x]$, $[P_z]$, and $[q_c + q_r + q_i + q_s + q_g]$, respectively, where

$$[F] = \sum_{i=1}^{512} \frac{1}{512} \int_0^{z_T} \bar{\rho} F_i dz,$$

and are shown in Figure 5. The time evolution of $[P_z]$ is in phase with that of $[q_c + q_r + q_i + q_s + q_g]$ as indicated by their correlation coefficient of 0.81, though more fluctuations occur in $[P_z]$ than in $[q_c + q_r + q_i + q_s + q_g]$. $[Px]$, however, does not follow the time evolution of $[qc + q_r + q_i + q_s + q_g]$, and their correlation coefficient is only 0.18. Thus the tendency of the vertical component of CVV is closely associated with the variation of tropical convection. Its tendency will be analyzed in the following discussion.

[11] To analyze the physical processes responsible for the variation of the vertical component of the CVV, the tendency equation for P_z is derived in Appendix A, which is expressed by

$$\frac{\partial P_z}{\partial t} = \underbrace{\left(-u\frac{\partial P_z}{\partial x} - w\frac{\partial P_z}{\partial z}\right) + \frac{\zeta}{\bar{\rho}}\left(\frac{\partial u}{\partial x}\frac{\partial \theta_e}{\partial x} + \frac{\partial w}{\partial x}\frac{\partial \theta_e}{\partial z}\right)}_{\text{Term A}}$$

$$+ \underbrace{\frac{1}{\bar{\rho}}\frac{\partial \theta_e}{\partial x}\frac{\partial B}{\partial x}}_{\text{Term B}} - \underbrace{\frac{L_f}{c_p}\frac{\zeta}{\bar{\rho}}\frac{\partial}{\partial x}\left(\frac{P_{18}\theta_e}{T}\right)}_{\text{Term M}} - \underbrace{\frac{1}{c_p}\frac{\zeta}{\bar{\rho}}\frac{\partial}{\partial x}\left(\frac{Q_R\theta_e}{T}\right)}_{\text{Term R}}. \quad (2)$$

In equation (2) the tendency of P_z is determined by five terms on the right-hand side. Term A includes the first two terms and is related to dynamic and thermodynamic processes including the zonal and vertical advection of P_z and the interaction between vorticity and the gradients of wind and equivalent potential temperature. Term B is the

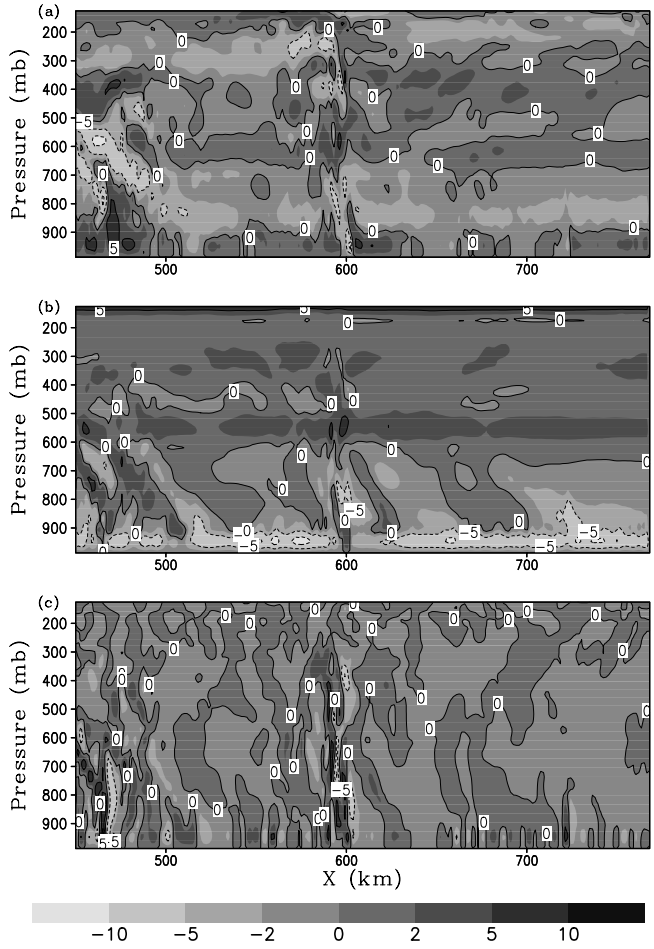

Figure 4. Zonal-vertical (X–Z) cross sections of (a) vorticity (10^{-3} s^{-1}), (b) $(\partial\theta_e)/\partial z$ (10^{-3} Km^{-1}), and (c) $-((\partial\theta_e)/\partial x)(2 \times 10^{-4}$ Km^{-1}) at 2100 LST 21 December 1992.

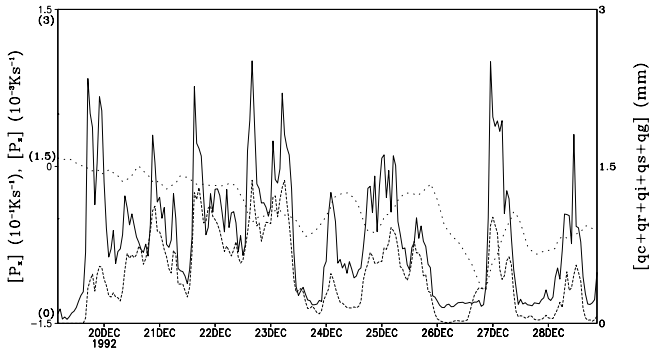

Figure 5. Time series of zonally averaged, mass-integrated zonal ($[P_x]$, $10^{-1}\mathrm{Ks}^{-1}$, dotted line) and vertical ($[P_z]$, $10^{-3}\mathrm{Ks}^{-1}$, solid line) components of the CVV, and sum of mixing ratios of cloud hydrometeors ($[q_c + q_r + q_i + q_s + q_g]$, mm, dashed line) during the 10-day integration. The plotting scales of $[P_x]$ and $[P_z]$ and $[q_c + q_r + q_i + q_s + q_g]$ are -0.15–0.15 Ks^{-1}, 0–$3 \times 10^{-3}\mathrm{Ks}^{-1}$, and 0–3 mm, respectively.

third term and is associated with the buoyancy force. Term M is the fourth term and is associated with cloud microphysical processes. Term R is the fifth term and includes the solar and infrared radiative forcing.

[12] The zonal mean and mass integration of equation (2) yields

$$\frac{\partial[P_z]}{\partial t} = \left[\frac{\zeta}{\bar{\rho}}\left(\frac{\partial u}{\partial x}\frac{\partial \theta_e}{\partial x} + \frac{\partial w}{\partial x}\frac{\partial \theta_e}{\partial z}\right)\right] + \left[\frac{1}{\bar{\rho}}\frac{\partial \theta_e}{\partial x}\frac{\partial B}{\partial x}\right] - \frac{L_f}{c_p}\left[\frac{\zeta}{\bar{\rho}}\frac{\partial}{\partial x}\left(\frac{P_{18}\theta_e}{T}\right)\right] - \frac{1}{c_p}\left[\frac{\zeta}{\bar{\rho}}\frac{\partial}{\partial x}\left(\frac{Q_R\theta_e}{T}\right)\right]. \quad (3)$$

The zonal mean and mass integration of the first term in equation (2) is much smaller than the other terms in equation (3) and is thus excluded in equation (3).

[13] To examine the processes responsible for the variation of $[P_z]$, time series of the four terms in the tendency equation (3) are plotted in Figure 6. [Term M] follows the tendency of $[P_z]$ closely in both phase and amplitude with a correlation coefficient of 0.97 and a root-mean-square (RMS) difference of 1.2×10^{-6} Ks^{-2}, which is much smaller than the standard deviation of the tendency of $[P_z]$ (3.7×10^{-6} Ks^{-2}). [Term B] is positive and has moderate amplitudes, whereas [Term A] is negative. Their correlation coefficients with the tendency of $[P_z]$ are smaller than 0.2, and their RMS differences with the tendency of $[P_z]$ are similar to the standard deviation of the tendency of $[P_z]$. [Term R] is negligible. Thus

$$\frac{\partial[P_z]}{\partial t} \approx -\frac{L_f}{c_p}\left[\frac{\zeta}{\bar{\rho}}\frac{\partial}{\partial x}\left(\frac{P_{18}\theta_e}{T}\right)\right]. \quad (4)$$

[14] The dominance of [Term M] in the variation of $[P_z]$ indicates that the variation of the vertical component of the CVV is controlled by the interaction between the vorticity and zonal gradient of cloud heating. Equation (A4b) shows that the cloud heating comes from the ice microphysical processes including vapor deposition, evaporation of liquid water from the surface of graupel, accretion of cloud water by snow, and melting of snow and graupel. This implies that P_{18} could be zero in water clouds. Thus the variation of the vertical component of the CVV is associated with the variation of the mixing ratios of ice clouds through the interaction between the dynamics and ice microphysics.

4. Summary

[15] A new vector $(\vec{\xi} \times \nabla\theta_e)/\rho$ (convective vorticity vector, CVV) is introduced to study tropical convection. In the 2-D x-z frame the CVV has two components: a zonal component associated with the product of the vorticity and the vertical gradient of equivalent potential temperature and a vertical component related to the product of the vorticity and the zonal gradient of equivalent potential temperature. Both components are calculated using hourly data from a 10-day, 2-D cloud-resolving simulation, which is forced by the vertical velocity, zonal wind, horizontal advection, and sea surface temperature observed and derived from the TOGA COARE.

[16] The analysis of zonally averaged and mass-integrated quantities shows that the variation of the vertical component of the CVV follows the variation of the sum of the mixing ratios of cloud hydrometeors with a correlation coefficient of 0.81, whereas the correlation coefficient between the zonal component of the CVV and the sum of the mixing ratios is 0.18. This indicates that the vertical component is a good indicator for the variation of 2-D tropical convection. The tendency equation for the vertical component of the CVV is derived to determine the dominant physical processes responsible for its variation. Analysis of the zonally averaged and mass-integrated tendency budget reveals that the interaction between the vorticity and zonal gradient of cloud heating accounts for the tendency of the vertical component of the CVV, indicating the interaction between dynamics and cloud microphysics links the CVV and clouds. The analysis further shows that the ice microphysics dominates the cloud heating, implying there are dynamic differences in CVV between water and ice clouds. Processes associated with buoyancy forcing and dynamic and thermodynamic interaction have a moderate impact on the tendency,

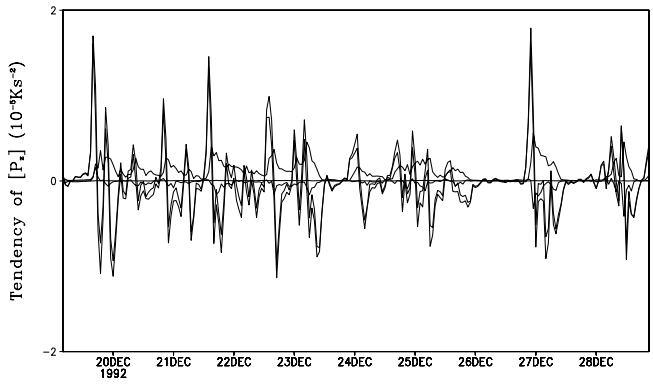

Figure 6. Time series of four contributing processes in the tendency equation for $[P_z]$ in equation (3) during the 10-day integration. Black, green, red, blue, and orange lines denote the tendency of $[P_z]$, [Term A], [Term B], [Term M], and [Term R], respectively. Units are in 10^{-5} Ks^{-2}. See color version of this figure at back of this issue.

whereas radiative processes have no significant effect. The preliminary, 2-D results suggest that the vertical component of the CVV is a cloud-related parameter that can be used to study the interaction among dynamic, thermodynamic, cloud microphysical processes during the development of 2-D tropical convection.

Appendix A: Derivation of Tendency Equation of P_z

[17] The zonal and vertical momentum equations can be expressed by

$$\frac{\partial u}{\partial t} = -u\frac{\partial u}{\partial x} - w\frac{\partial u}{\partial z} - c_p\frac{\partial(\bar{\theta}\pi)}{\partial x}, \tag{A1a}$$

$$\frac{\partial w}{\partial t} = -u\frac{\partial w}{\partial x} - w\frac{\partial w}{\partial z} - c_p\frac{\partial(\bar{\theta}\pi)}{\partial z} + B, \tag{A1b}$$

where $\pi = (p/p_o)^{\kappa}$ with $\kappa = R/c_p$; R is the gas constant; c_p is the specific heat of dry air at constant pressure p, and p_o = 1000 mb; $B = g(\frac{\theta'}{\theta_b} + 0.61q_v - q_c - q_r - q_i - q_s - q_g)$ is the buoyancy force, and q_v is the specific humidity. An overbar denotes a zonal mean and subscript b denotes an initial value, which does not vary with time. A prime is the perturbation from the zonal mean. The dissipation terms are excluded in equation (A1) for simplicity.

[18] Taking $\partial/\partial z$ (equation (A1a)) $- \partial/\partial z$ (equation (A1b)) and using mass continuity equation, the tendency equation for the vorticity ζ in an elastic approximation as is used in the two-dimensional (2-D) cloud-resolving model is expressed by

$$\frac{\partial}{\partial t}\left(\frac{\zeta}{\bar{\rho}}\right) = -u\frac{\partial}{\partial x}\left(\frac{\zeta}{\bar{\rho}}\right) - w\frac{\partial}{\partial z}\left(\frac{\zeta}{\bar{\rho}}\right) - \frac{1}{\bar{\rho}}\frac{\partial B}{\partial x}. \tag{A2}$$

Here $\bar{\rho}$ is the mean air density and is a function of height only.

[19] The tendency equations for potential temperature and specific humidity are

$$\frac{\partial \theta}{\partial t} = -u\frac{\partial \theta}{\partial x} - w\frac{\partial \theta}{\partial z} + \frac{Q_{cn}}{\pi c_p} + \frac{Q_R}{\pi c_p}, \tag{A3a}$$

and

$$\frac{\partial q_v}{\partial t} = -u\frac{\partial q_v}{\partial x} - w\frac{\partial q_v}{\partial z} - S_{qv}, \tag{A3b}$$

where

$$\begin{aligned} Q_{cn} = {} & L_v(P_{CND} - P_{REVP}) + L_s\{P_{DEP} + (1-\delta_1)P_{SDEP}(T < T_o) \\ & + (1-\delta_1)P_{GDEP}(T < T_o) - P_{MLTS}(T > T_o) \\ & - P_{MLTG}(T > T_o)\} + L_f\{P_{SACW}(T < T_o) + P_{SFW}(T < T_o) \\ & + P_{GACW}(T < T_o) + P_{IACR}(T < T_o) + P_{GACR}(T < T_o) \\ & + P_{SACR}(T < T_o) + P_{GFR}(T < T_o) - P_{RACS}(T > T_o) \\ & - P_{SMLT}(T > T_o) - P_{GMLT}(T > T_o) + P_{IHOM}(T < T_{oo}) \\ & - P_{IMLT}(T > T_o) + P_{IDW}(T_{oo} < T < T_o)\}, \end{aligned} \tag{A3c}$$

and

$$\begin{aligned} S_{qv} = {} & P_{CND} - P_{REVP} + P_{DEP} + (1-\delta_1)P_{SDEP}(T < T_o) \\ & + (1-\delta_1)P_{GDEP}(T < T_o) - P_{MLTS}(T > T_o) \\ & - P_{MLTG}(T > T_o). \end{aligned} \tag{A3d}$$

Here, T is air temperature, and $T_o = -35°C$. L_v, L_s, and L_f are latent heat of vaporization, sublimation, and fusion at 0°C, respectively, and $L_s = L_v + L_f$. Q_R is the radiative heating rate due to convergence of the net flux of solar and infrared radiative fluxes. P_{CND} is the growth rate of cloud water by the condensation of supersaturated vapor. P_{DEP}, P_{SDEP}, and P_{GDEP} are the growth rates of cloud ice, snow, and graupel by the deposition of supersaturated vapor, respectively. P_{REVP} is the growth rate of vapor by the evaporation of rain. P_{MLTS} and P_{MLTG} are the growth rates of vapor by the evaporation of melting snow and liquid water from the surface of graupel, respectively. P_{IMLT} is the growth rate of cloud water by the melting of cloud ice. P_{GMLT}, P_{SMLT}, and P_{RACS} are the growth rates of rain by the melting of snow and graupel and accretion of snow, respectively. P_{IDW}, P_{IACR}, and P_{IHOM} are the growth rates of cloud ice by the deposition of cloud water, accretion of rain, and homogeneous freezing of cloud water, respectively. P_{SACW}, P_{SFW}, and P_{SACR} are the growth rates of snow by the accretion and deposition of cloud water and accretion of rain, respectively. P_{GACR}, P_{GACW}, and P_{GFR} are the growth rates of graupel by the accretion of rain and cloud water and freezing of rain, respectively. The parameterized schemes for these cloud microphysical processes are from *Rutledge and Hobbs* [1983, 1984], *Lin et al.* [1983], *Tao et al.* [1989], and *Krueger et al.* [1995], which are summarized in the works of *Tao and Simpson* [1993] and *Li et al.* [1999, 2002c].

[20] Taking

$$\frac{1}{\theta} \times (\text{A3a}) + \frac{L_v}{c_p T} \times (\text{A3b})$$

and defining the equivalent potential temperature θ_e as $\theta \exp((L_v q_v)/(c_p T))$ yields a tendency equation for equivalent potential temperature given by

$$\frac{\partial \theta_e}{\partial t} = -u\frac{\partial \theta_e}{\partial x} - w\frac{\partial \theta_e}{\partial z} + \frac{L_f}{c_p}\frac{P_{18}\theta_e}{T} + \frac{1}{c_p}\frac{Q_R\theta_e}{T}, \tag{A4}$$

where

$$\begin{aligned} P_{18} = {} & P_{DEP} + (1-\delta_1)P_{SDEP}(T < T_o) + (1-\delta_1)P_{GDEP}(T < T_o) \\ & - P_{MLTS}(T > T_o) - P_{MLTG}(T > T_o) + P_{SACW}(T < T_o) \\ & + P_{SFW}(T < T_o) + P_{GACW}(T < T_o) + P_{IACR}(T < T_o) \\ & + P_{GACR}(T < T_o) + P_{SACR}(T < T_o) + P_{GFR}(T < T_o) \\ & - P_{RACS}(T > T_o) - P_{SMLT}(T > T_o) - P_{GMLT}(T > T_o) \\ & + P_{IHOM}(T < T_{oo}) - P_{IMLT}(T > T_o) \\ & + P_{IDW}(T_{oo} < T < T_o). \end{aligned} \tag{A4a}$$

The term

$$-\frac{L_v}{c_p}\frac{\theta_e q_v}{T^2}\left(\frac{\partial T}{\partial t}+\frac{\partial T}{\partial x}+w\frac{\partial T}{\partial z}\right)$$

is omitted in the derivation of equation (A4) since it is much smaller than the other terms in equation (A4). Based on *Li et al.* [2002c], P_{18} in a tropical, deep convective regime can be simplified as

$$P_{18} = P_{DEP} - P_{MLTG}(T > T_o) + P_{SACW}(T < T_o) - P_{SMLT}(T > T_o) - P_{GMLT}(T > T_o). \quad \text{(A4b)}$$

[21] Taking

$$-\frac{\partial \theta_e}{\partial x}\times(\text{A2}) - \frac{\zeta}{\bar{\rho}}\frac{\partial(\text{A4})}{\partial x},$$

the tendency equation for the vertical component of the CVV

$$P_z = -\frac{\zeta}{\bar{\rho}}\frac{\partial \theta_e}{\partial x}$$

can be expressed by

$$\frac{\partial P_z}{\partial t} = \left(-u\frac{\partial P_z}{\partial x} - w\frac{\partial P_z}{\partial z}\right) + \frac{\zeta}{\bar{\rho}}\left(\frac{\partial u}{\partial x}\frac{\partial \theta_e}{\partial x} + \frac{\partial w}{\partial x}\frac{\partial \theta_e}{\partial z}\right) + \frac{1}{\bar{\rho}}\frac{\partial \theta_e}{\partial x}\frac{\partial B}{\partial x} - \frac{L_f}{c_p}\frac{\zeta}{\bar{\rho}}\frac{\partial}{\partial x}\left(\frac{P_{18}\theta_e}{T}\right) - \frac{1}{c_p}\frac{\zeta}{\bar{\rho}}\frac{\partial}{\partial x}\left(\frac{Q_R\theta_e}{T}\right). \quad \text{(A5)}$$

[22] **Acknowledgments.** Authors thank M. Zhang at the State University of New York, Stony Brook for his TOGA COARE forcing data, S. Lang at NASA/GSFC for his editorial assistance, and an anonymous reviewer for comments. S. Gao and F. Ping are supported by the National Natural Sciences Foundation of China under the grants 40333028 and 40305010. X. Li is supported by the Joint Center for Satellite Data Assimilation. W.-K. Tao is supported by the NASA Headquarters Atmospheric Dynamics and Thermodynamics Program and the NASA Tropical Rainfall Measuring Mission (TRMM). The author is grateful to R. Kakar at NASA headquarters for his support.

References

Bennetts, D. A., and B. J. Hoskins (1979), Conditional symmetric instability- a possible explanation for frontal rainbands, *Q. J. R. Meteorol. Soc.*, *105*, 945–962.

Cao, Z., and H. Cho (1995), Generation of moist vorticity in extratropical cyclones, *J. Atmos. Sci.*, *52*, 3263–3281.

Cho, H., and Z. Cao (1998), Generation of moist vorticity in extratropical cyclones, part II: Sensitivity to moisture distribution, *J. Atmos. Sci.*, *55*, 595–610.

Danielsen, E. F., and R. S. Hipskind (1980), Stratospheric-tropospheric exchange at polar latitudes in summer, *J. Geophys. Res.*, *85*, 393–400.

Emanuel, K. A. (1979), Inertial instability and mesoscale convective systems. Part I: Linear theory of inertial instability in rotating viscous fluids, *J. Atmos. Sci.*, *36*, 2425–2449.

Ertel, H. (1942), Ein neuer hydrodynamischer wirbelsatz, *Meteorol. Zeitschr Braunschweigs*, *6*, 277–281.

Gao, S.-T., T. Lei, and Y.-S. Zhou (2002), Moist potential vorticity anomaly with heat and mass forcings in torrential rain system, *Chin. Phys. Lett.*, *19*, 878–880.

Grabowski, W. W., X. Wu, and M. W. Moncrieff (1996), Cloud-resolving model of tropical cloud systems during Phase III of GATE. Part I: Two-dimensional experiments, *J. Atmos. Sci.*, *53*, 3684–3709.

Hoskins, B. J., and P. Berrisford (1988), A potential vorticity perspective of the storm of 15–16 October 1987, *Weather*, *43*, 122–129.

Krueger, S. K., Q. Fu, K. N. Liou, and H.-N. S. Chin (1995), Improvement of an ice-phase microphysics parameterization for use in numerical simulations of tropical convection, *J. Appl. Meteorol.*, *34*, 281–287.

Li, X. (2004), Cloud modeling in the tropical deep convective regime, in *Observation, Theory, and Modeling of Atmospheric Variability*, edited by X. Zhu, pp. 206–223, World Sci., River Edge, N. J.

Li, X., C.-H. Sui, K.-M. Lau, and M.-D. Chou (1999), Large-scale forcing and cloud-radiation interaction in the tropical deep convective regime, *J. Atmos. Sci.*, *56*, 3028–3042.

Li, X., C.-H. Sui, and K.-M. Lau (2002a), Precipitation efficiency in the tropical deep convective regime: A 2-D cloud resolving modeling study, *J. Meteorol. Soc. Jpn.*, *80*, 205–212.

Li, X., C.-H. Sui, and K.-M. Lau (2002b), Interactions between tropical convection and its environment: An energetics analysis of a 2D cloud resolving simulation, *J. Atmos. Sci.*, *59*, 1712–1722.

Li, X., C.-H. Sui, and K.-M. Lau (2002c), Dominant cloud microphysical processes in a tropical oceanic convective system: A 2-D cloud resolving modeling study, *Mon. Weather Rev.*, *130*, 2481–2491.

Lin, Y.-L., R. D. Farley, and H. D. Orville (1983), Bulk parameterization of the snow field in a cloud model, *J. Clim. Appl. Meteorol.*, *22*, 1065–1092.

Montgomery, M. T., and B. F. Farrell (1993), Tropical cyclone formation, *J. Atmos. Sci.*, *50*, 285–310.

Rutledge, S. A., and P. V. Hobbs (1983), The mesoscale and microscale structure and organization of clouds and precipitation in midlatitude cyclones. Part VIII: A model for the "seeder-feeder" process in warm-frontal rainbands, *J. Atmos. Sci.*, *40*, 1185–1206.

Rutledge, S. A., and P. V. Hobbs (1984), The mesoscale and microscale structure and organization of clouds and precipitation in midlatitude cyclones. Part XII: A disgnostic modeling study of precipitation development in narrow cold-frontal rainbands, *J. Atmos. Sci.*, *41*, 2949–2972.

Soong, S. T., and Y. Ogura (1980), Response of tradewind cumuli to large-scale processes, *J. Atmos. Sci.*, *37*, 2035–2050.

Soong, S. T., and W.-K. Tao (1980), Response of deep tropical cumulus clouds to Mesoscale processes, *J. Atmos. Sci.*, *37*, 2016–2034.

Sui, C.-H., K. M. Lau, W.-K. Tao, and J. Simpson (1994), The tropical water and energy cycles in a cumulus ensemble model. Part I: Equilibrium climate, *J. Atmos. Sci.*, *51*, 711–728.

Sui, C.-H., X. Li, and K.-M. Lau (1998), Radiative-convective processes in simulated diurnal variations of tropical oceanic convection, *J. Atmos. Sci.*, *55*, 2345–2359.

Tao, W.-K., and J. Simpson (1993), The Goddard Cumulus Ensemble model. Part I: Model description, *Terr. Atmos. Oceanic Sci.*, *4*, 35–72.

Tao, W.-K., J. Simpson, and M. McCumber (1989), An ice-water saturation adjustment, *Mon. Weather Rev.*, *117*, 231–235.

Thorpe, A. J. (1985), Diagnosis of balanced vortex structure using potential vorticity, *J. Atmos. Sci.*, *42*, 397–406.

Weller, R. A., and S. P. Anderson (1996), Surface meteorology and air-sea fluxes in the western equatorial Pacific warm pool during TOGA COARE, *J. Climate*, *9*, 1959–1990.

Wu, X., W. W. Grabowski, and M. W. Moncrieff (1998), Long-term evolution of cloud systems in TOGA COARE and their interactions with radiative and surface processes. Part I: Two-dimensional cloud-resolving model, *J. Atmos. Sci.*, *55*, 2693–2714.

Xu, K.-M., and D. A. Randall (1996), Explicit simulation of cumulus ensembles with the GATE Phase III data: Comparison with observations, *J. Atmos. Sci.*, *53*, 3710–3736.

Xu, Q. (1992), Formation and evolution of frontal rainbands and geostrophic potential vorticity anomalies, *J. Atmos. Sci.*, *49*, 629–648.

Zhang, M. H., and J. L. Lin (1997), Constrained variational analysis of sounding data based on column-integrated budgets of mass, heat, moisture, and momentum: Approach and application to ARM measurements, *J. Atmos. Sci.*, *54*, 1503–1524.

S. Gao and F. Ping, LACS, Institute of Atmospheric Physics, Chinese Academy of Sciences, Beijing 100029, China. (gst@lasg.iap.ac.cn; pingf@mail.iap.ac.cn)

X. Li, 11876 Tall Timber Drive, Clarksville, MD 21029, USA. (xiaofan.li@noaa.gov)

W.-K. Tao, Laboratory for Atmospheres, NASA Goddard Space Flight Center, Greenbelt, MD 20771, USA. (tao@agnes.gsfc.nasa.gov)

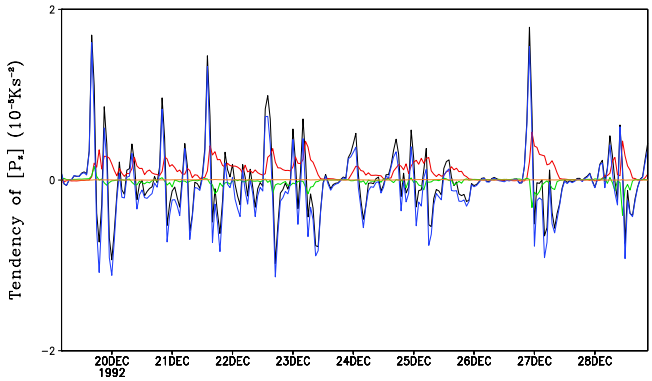

Figure 6. Time series of four contributing processes in the tendency equation for $[P_z]$ in equation (3) during the 10-day integration. Black, green, red, blue, and orange lines denote the tendency of $[P_z]$, [Term A], [Term B], [Term M], and [Term R], respectively. Units are in 10^{-5} Ks^{-2}.